Effects of In-Mold Additions of Al, Ca, Ce, Sr, or Ti on Austenite Grain Morphology and Eutectic Cell Size of a Hypoeutectic Gray Cast Iron

Evan J. Carter, Jingjing Qing, Mingzhi Xu
Georgia Southern University, Statesboro, Georgia, USA

ABSTRACT

Effects of different in-mold additions on the morphology of austenite and the eutectic cell structure in gray iron were investigated using a hypoeutectic gray iron. Direct Austempering After Solidification (DAAS) heat treatment was adopted to retain the grain boundaries of austenite at room temperature in a gray iron alloyed with Ni, Mo and Cu. The additions studied included Al, Ca, Ce (added as mischmetal), Sr, and Ti. In a single heat, each addition was added into individual mold cavities prior to pouring of the gray iron at 0.05%. The austenite grain boundaries and the eutectic cell structures were revealed with chemical etching. The results indicated that the Sr was most effective on refining austenite at the tested addition rate. Meanwhile, Al had the least refined structure with the largest grains and the fewest grains. Additionally, it was found that larger equiaxed zones had larger eutectic cells.

Keywords: in-mold addition, austenite, hypoeutectic gray iron, direct austempering after solidification, DAAS, eutectic cell, grain refinement

INTRODUCTION

CAST/GRAY IRON

Cast iron (CI) is the iron-carbon-silicon (Fe-C-Si) alloy with a carbon content of 2.1 *wt. %* or higher. Gray iron (GI) is a sub-class of cast iron that is characterized by the presence of flake graphite in the microstructure. Figure 1 is a stable iron-carbon phase diagram. Several of the phases that will be referenced later are present in the phase diagram, such as: austenite (γ), ferrite (α), and graphite (Gr).[1] Additionally, the diagram shows phase transformations and phase composition ranges in phases of the iron-carbon system. For example, the carbon solubility limit in austenite is 2.1 wt.% (0.021 in fraction). The eutectic point is also shown at 4.3 wt.% carbon. The horizontal line at ~1153C (2107F), starting at the austenite phase field, indicates the threshold for eutectic transformation.

Upon solidification, following the stable Fe-C phase diagram, graphite may precipitate, which produces the graphitic cast irons. In gray iron, graphite precipitates as networks of flake structures within an iron matrix.

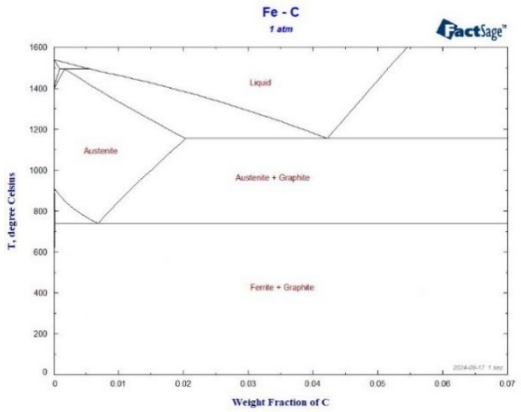

Figure 1. The stable iron-carbon phase diagram.

The interconnected network of graphite flakes in gray iron leads to excellent machinability, thermal conductivity, and vibration dampening capabilities.[2] The microstructure can be observed optically on a polished sample of gray iron. Figure 2 is an un-etched micrograph of gray iron.[3]

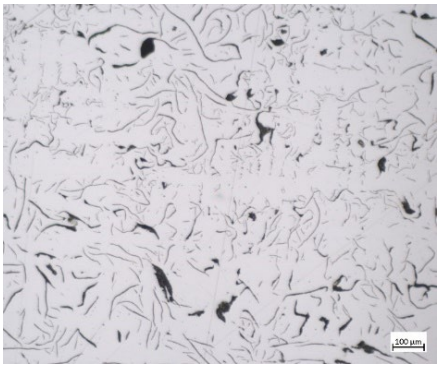

Figure 2. A micrograph of unetched gray iron.

AUSTENITE

Austenite is the face-centered cubic (FCC) crystal structure of iron and is the first solid formed from the liquid during the solidification of a hypoeutectic cast iron. Austenite form as dendrites in liquid. Dendrites are characterized by their tree-like shape. The shape results from the initial growth of a larger primary

dendrite that serves as a substrate for secondary dendrite arms along its sides.[4]

In equilibrium conditions, austenite is stable above the eutectoid temperature and will transform into ferrite and graphite at lower temperatures. In common cast iron alloys, unless they are stabilized with alloys or heat treatments, austenite will transform to other phases such as pearlite and martensite. The phases that austenite transforms into will depend on alloying elements and cooling conditions.[1,5]

EUTECTIC GROWTH AND EUTECTIC CELLS

In gray iron, the presence of eutectic cells is a result of the formation of eutectic austenite and graphite during the eutectic reaction. Once eutectic solidification has started, eutectic graphite will begin to nucleate and grow. The growth of eutectic graphite will begin at a nucleation site and cause graphite flakes to expand outwards. Below eutectic temperatures, the solubility of carbon in austenite decreases with continues cooling. Carbon will be rejected from austenite into the adjacent graphite to further the graphite growth.[6,7] Figure 3 depicts the development of eutectic cells in hypoeutectic gray iron.[6] Eutectic cells often nucleate on primary dendrites due to the solute rich liquid which develops around them from the rejection of carbon. Therefore, primary austenite grains can affect the orientation of the eutectic austenite. However, it is possible for eutectic cells to grow independently with no dependency on primary austenite.[6,8]

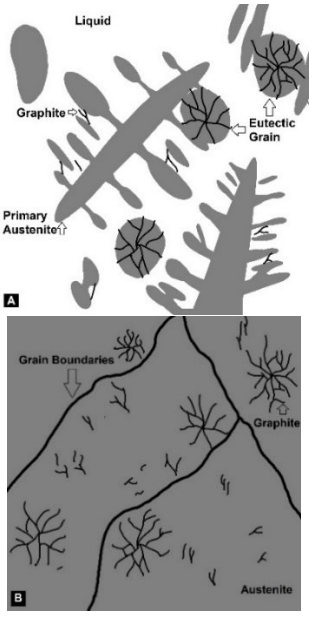

Figure 3. A depiction of eutectic solidification in gray iron. (A) Hypoeutectic alloy, early solidification. (B) Hypoeutectic alloy, late solidification. Figures redrawn from Reference 7.

GRAIN MORPHOLOGY/REFINEMENT

On a casting cross section, three zones with different grain morphology are generally distinguished: equiaxed, columnar, and chill zones, as demonstrated in Figure 4. The chill zone is made of fine equiaxed grains because of fast cooling rates at the casting to mold interface. The chill grains experienced minimal growth when compared to equiaxed and columnar grains. Elongated columnar grains are observed next to the chill zone and grow inward, and the length directions follows the thermal gradient. Further toward the center of the casting, equiaxed grains are much more isotropic in dimension compared to the columnar grains. The size of grains can indicate how refined the grain structure is. Grain refinement leads to smaller sized grains. The mechanism behind refinement can vary, but, in general, a finer structure is preferred due to the positive correlation it has with improving the strength of a casting.[9,10]

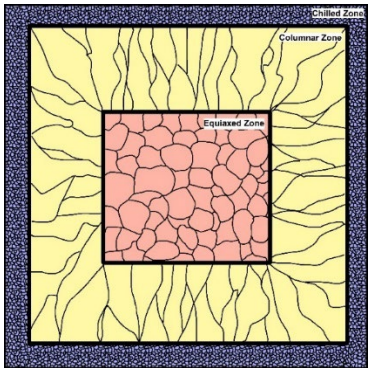

Figure 4. A diagram of the various grain structures that are present in castings. Red highlights the equiaxed grains. Yellow highlights are columnar grains, and blue highlights are chilled grains. Figure redrawn from Reference 9.

DIRECT AUSTEMPERING AFTER SOLIDIFICATION

Direct austempering after solidification (DAAS) is a heat-treatment process that retains austenite grain structures in a cast iron by forming ausferrite. Ausferrite is made of acicular ferrite and retained carbon-rich austenite. The ausferrite microstructure is achieved via isothermal transformation of austenite, normally in molten salt bath. The orientation of the retained austenite should be inherited from the initial orientation of primary austenite. This allows for the observation of austenite grain structures. The eutectic cell made of austenite and graphite was not reconstructed, so its grain structure is also retained. Observation of austenite microstructures is possible after DAAS heat-treatment, polishing and etching. Chemical etching helps to highlight the eutectic cell structures. The specific heat-treatment steps and etching methods will be described in later sections.[7,11,12]

OBJECTIVE AND IMPACT

The objective of this research is to compare the effects of selected additions on morphology of austenite grains in gray iron. The gray iron used in this study was alloyed with Ni, Cu, and Mo to stabilize the ausferrite microstructure during DAAS process. The quantification and characterization of austenite grains are based on experimental observations instead of approximation.

DESIGN OF EXPERIMENTS

Five different additions were studied and compared, including the misch metal with cerium (Ce) and four elemental additions: aluminum (Al), calcium (Ca), strontium (Sr), and titanium (Ti). Chemical compositions of all additions are listed in the later section. The additions were added into separate mold cavities (resting at the bottom of the drag impression) at roughly 0.05 wt.%, based on casting weight. Specifically, the amount of the addition used was calculated off the weight of a bar excluding the gating system, referenced in the "Casting/Molds" section of this paper.

High-purity Si was added in-ladle during tap to mimic the rise in Si content that would be seen from a common in-ladle FeSi inoculant treatment. High-purity Si was added in-ladle at 0.15 *wt.%* of the charge to decern the effect of the in-mold additions without the impact of an inoculant. Inoculant was not used in the experimental heat since it generally contains the elements that are to be studied in the present research. Specifically, the high purity Si was chosen for its low amount of Ca and Al impurities. With this choice, the inoculation process of producing gray iron can be more accurately represented while focusing on the effect of the in-mold additions.

CASTING/MOLDS

The design of the castings and molds used for this study was guided by the ASTM A48 standard for gray iron tensile bars. Figure 5 shows the schematics for the bar castings and the molds used to produce the castings. The purple color area in Figure 5 indicates the volume for the mold. The filter is used to remove dross and inclusions. Based on the ASTM standard, specifications on bar dimensions, inlet dimensions, mold wall thickness, pouring basin size, and pouring basin location were followed while designing the mold.[13] Mold walls in the drag are not thinner than the maximum diameter of the bar. The inlet is a cylinder of 3/16 in. (4.8 mm) in height and 1/8 in. (3.2 mm) in diameter. The resulting design was a top-fill gating system with a mold cavity for the bar in the drag and the pouring basin impression in the cope. In addition, a 10-ppi ceramic filter was added to the bottom of the pouring basin and a thermocouple (TC) was installed to each mold (location indicated in green in Figure 5). The molds were made of a nobake sand mixture that has 1.5 wt.% phenolic-urethane resin and 35.0 wt.% co-reactant to resin.

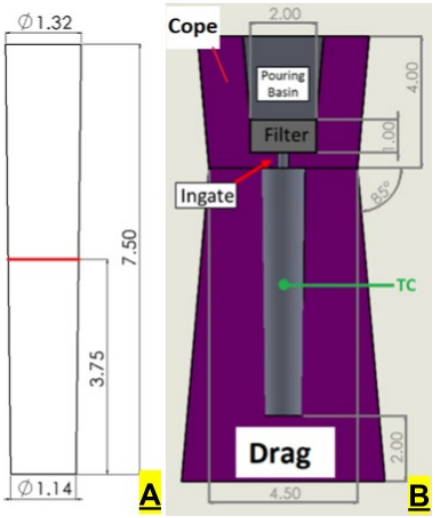

Figure 5. (A) A schematic of the bar. (B). A schematic of the mold with labels for the various parts. The dimensions are in inches.

HEAT PROCEDURE

The charge materials used include high-purity pig iron, steel scrap, graphite, ferrosilicon, ferromanganese, ferromolybdenum, nickel, and iron sulfide. The charge material was open-air melted in a 100-lb. medium-frequency coreless induction furnace. After the charge materials became fully liquid, the chemistry of the metal in the furnace was measured and adjusted before the melt temperature reached 1530C (2786F). Afterwards, the melt was held at 1505C (2741F) for 10 minutes. This hold in air was used to ensure that equilibrium levels of oxygen/nitrogen were reached in the metal and all additions for chemistry adjustment were dissolved.

After the hold at 1505C (2741F), the molten metal was tapped into a preheated 100-lb. teapot transfer ladle with the high-purity Si addition at the bottom. Another chemistry sample was then taken from the ladle, and the chemistry of the sample is shown in Table 1. Afterwards, the five molds with individual additions were poured. The cooling curve of each mold was tracked using a Data Acquisition system and monitored for the subsequent DAAS heat treatment.

DAAS HEAT-TREATMENT PROCEDURE

The DAAS heat-treatment begins with an interrupted solidification step, after the iron was poured in the mold and during its solidification. A thermocouple is installed in the mold cavity, which will measure the temperature of the center of the casting. Once the

castings reach 1050C (1922F), they are shaken out of the mold and transferred to an air oven and held for 30 minutes. It should be noted that the inlet served as a break point for the casting. Therefore, only the bar itself underwent heat treatment. The air oven homogenizes the temperature throughout the bars to 1100C (2012F). The homogenized bars are then quenched and held in a salt bath at 260C (500F). During this isothermal cycle, austenite transforms to ausferrite. Additionally, the bars are held in the salt bath for four hours to ensure complete transformation throughout the entire casting. Figure 6 is a graph of thermal cycle over the duration of the DAAS heat-treatment process. After the isothermal hold, the castings were removed and air cooled.

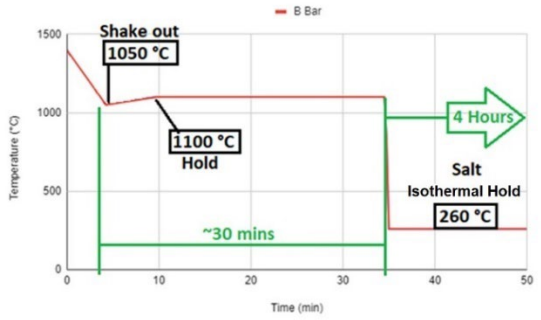

Figure 6. A graph of the approximate casting temperature over the DAAS heat-treatment process time. The red line indicates the temperature while the green and black indicate key steps of the treatment.

ALLOY CHEMISTRY & ADDITION CHEMISTRY

The gray iron alloy used in this research is hypoeutectic. A hypoeutectic alloy was chosen due to the presence of primary austenite present in comparison to eutectic austenite. Nickel and Mo are added to the chemistry to stabilize ausferrite during DAAS. The delayed transformation due to Ni and Mo additions allowed for more time to transfer the castings from the mold and into the air ovens. The measured chemical composition of the gray iron alloy is recorded in Table 1. The carbon and sulfur values were measured using a carbon sulfur combustion analyzer while the other values were measured with an optical emissions spectrometer (OES). The chemistry of the individual in-mold additions is listed in Tables 2-7. Each addition was added at 0.05 wt.% of the casting weight. It should be noted that content of addition element may be lower than 0.05 wt.% in the casting, depending on the actual recovery. Chemistry was not analyzed for each casting bar.

Table 1. Chemical Composition (wt.%) of Gray Iron Alloy

C	S	Si	P	Mn	Mo	Ni	Cu	Al	Ti
3.340	0.086	1.990	0.015	0.590	0.460	1.070	0.036	0.004	0.015

Table 2. Chemical Composition (wt%) of High-purity Si

Si	Ca	Al
99.347	0.087	0.103

Table 3. Chemical Composition (wt.%) of Al Addition

Al	Cu	Ni	Si	Mg	Cd	Fe	Cr	Pb
99.400	0.040	0.020	0.010	0.040	0.020	0.030	0.010	0.020

Table 4. Chemical Composition (wt.%) of Ca Addition

Ca	N	Mg	Si	Al	Cu	Cl	Mn	Ni	Fe
97.000	0.000	0.500	0.000	0.500	0.005	0.000	0.050	0.005	0.050

Table 5. Chemical Composition (wt.%) of Mischmetal Addition

La	Ce	C	Fe	Si	Mg	Mo	Ni	Al
35.000	65.000	0.030	0.200	0.040	0.100	0.030	0.000	0.000

Table 6. Chemical Composition (wt.%) of Sr Addition

Sr	Ba	Ca
99.500	0.180	0.0900

Table 7. Chemical Composition (wt.%) of Ti Addition

Ti	C	S	Al	P	V	Fe
70.750	0.160	0.020	4.730	0.020	2.710	21.610

ANALYSIS METHODS

SAMPLE PREPARATION

Figure 5a shows the dimensions of the bar castings and has a red line drawn across the width at half the length of the bar. The red line indicates the location where the castings were sectioned for analysis. The sectioning produced samples with a circular cross-section for polishing and etching. No material was removed from the surface of the casting, preserving the initial edges of the circular cross-sections. The sectioned surface was prepared with grinding steps ending at 1200 grit with SiC paper and was then polished with 0.1-micron alumina compound. An auto-polishing machine was utilized to increase reliability and accuracy of the grinding/polishing steps. After

polishing, 5% Nital etchant was used to reveal both the austenite grains and eutectic cells. The time for etching was 30 secs or longer (until the austenite grains were visible to the naked eye). It should be noted that different light source angles will show the austenite grains or eutectic cells at various clarities.

AUSTENITE GRAIN OBSERVATION AND CHARACTERIZATION

Austenite - Macrograph Capture Method

Revealing the austenite grains required a single diffused light source roughly 36 in. (900 mm) away and placed at an angle that is neither parallel nor normal to the viewing plane. The exact angle must be experimentally varied until a clear contrast between grains is seen. Other light sources were minimized, and images were taken with a black background in a dark room. A high-resolution DSLR camera (with 100mm f/2.8L IS ultrasonic motor (USM) macro lens) was used, and three images were taken for each sample from a top-down view. Each image varied the light's incoming angle radially around the sample and all three were used for image processing. Figure 7 is an example of one of the images taken to reveal austenite grain boundaries. The red, green, and blue (RGB) colors were filtered from each image and overlayed to further clarify the grain boundaries. Figure 8 is an example of the same sample after the three images have been overlaid and processed, and austenite grains have been identified/outlined.

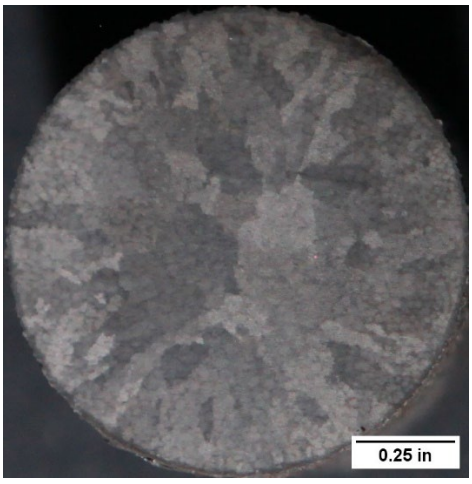

Figure 7. An example of an image taken to show the primary austenite grains. The image is unprocessed.

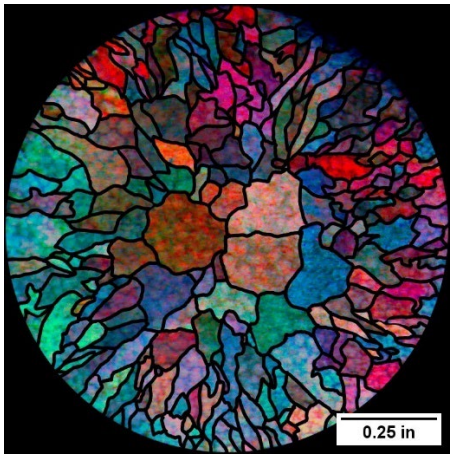

Figure 8. An example of the identified austenite grains after full image processing for the sample in Figure 7.

Austenite Grain Characterization

The austenite grains were first identified as either in the columnar zone or in the equiaxed zone. Columnar grains are identified as grains that are longer in length than width, nucleate near the mold wall, and grow inwards towards the center. By comparison, equiaxed grains have an aspect ratio closer to one and nucleate near the center of the casting. Once identified, the two different types can be analyzed separately. Figure 9 is an example of the sample from Figures 7-8 with the columnar grains shaded black.

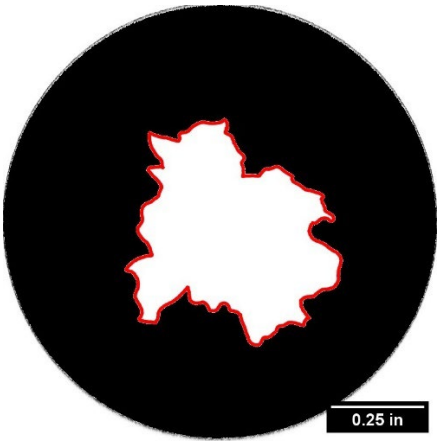

Figure 9. An example of the determined equiaxed zone (center white area) and columnar zone (black area). The sample is the same as in Figures 7-8.

An image processing software was used to count and measure the austenite grains. The austenite grains are quantified based on average area (in^2) (separated by type), columnar length, and equiaxed area percentage. The equiaxed area percentage is determined for each sample, indicating how much of the sectioned area is

equiaxed. Values for equiaxed area percentage is calculated following Eqn. 1,

$$Equiaxed\ Area\ \% = \frac{EG_{Tot.Area}}{CS_{Area}} \times 100 \qquad \textbf{Eqn. 1}$$

Where:
$EG_{Tot\ Area}$ = area of equiaxed grains; and
CS_{Area} = area of the cross section.

Average columnar length is calculated based on the total section area and area of equiaxed grains. Average columnar grain length can be calculated by subtracting the radius of the cross-section by the radius of an equivalent circle whose area equals the total area of equiaxed grains. Equation 2 shows the calculation for the radius of a circle using the area of the equiaxed zone. Equation 3 shows the calculation of the average columnar length (Avg. Col. Length). Figure 10 shows the geometrical calculation being used to represent average columnar length.

$$r_{equiaxed\ area} = \sqrt{\frac{Area_{Equiaxed\ Grains}}{\pi}} \qquad \textbf{Eqn. 2}$$

$$Avg.Col.Length = r_{CS} - r_{equiaxed\ area} \qquad \textbf{Eqn. 3}$$

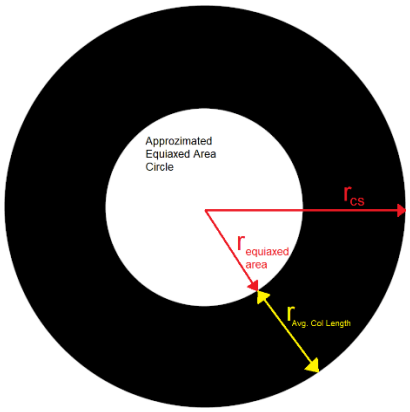

Figure 10. A figure showing how the average columnar length was calculated. Long red line: cross-section radius. Short red line: equiaxed area radius. Yellow line: average columnar length.

EUTECTIC CELL OBSERVATION AND CHARACTERIZATION

Eutectic Cell - Macrograph Capture Method

A similar dark room environment was used to increase the contrast of the eutectic cells when observed with a single light source. The same diffused light source was situated 2-3 in. (50-75 mm) from the surface of the sample. The high-resolution camera was used to capture an image of the surface. Figure 11 is an example of an image taken to highlight the eutectic cells. In this image, a micro-ruler and scale bar are included. Additionally, lines are present that were added to aid the analysis of the eutectic cells, explained in a later section.

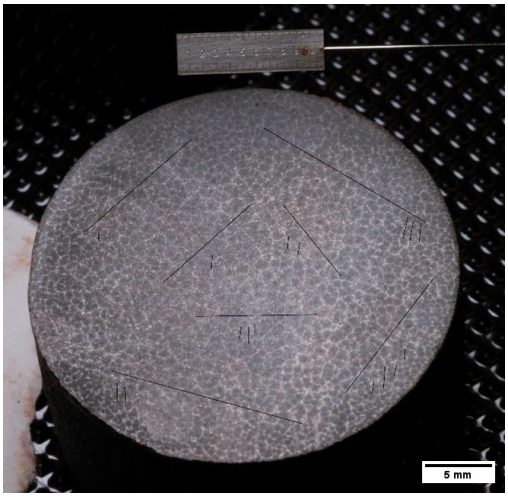

Figure 11. An example of the images taken of the eutectic cells. A scale bar is included to indicate 5mm (0.2 in.). The lines present were added/used for measuring the size of the eutectic cell diameter. Note that the image was not captured normal to the plane of polish for a better contrast of eutectic cells, and thus the sample section appears elliptical.

Eutectic Cell Characterization

The eutectic cells were characterized by the average diameter. The size of the eutectic cells was calculated using the mean linear intercept method. Lines were drawn over the cross-section as shown in Figure 11. The average diameter of the eutectic cells was found by dividing the length of the line by the number of intercepting eutectic cells. Additionally, the value was averaged from three measurements for both the equiaxed zone and the columnar zone. Utilizing this process, separate values for the equiaxed zone and the columnar zone can be found.

RESULTS AND DISCUSSION

AUSTENITE

The austenite grain boundaries were successfully revealed in the castings that underwent the DAAS heat-treatment process. The grains are visible without magnification but lack clarity without the imaging process performed. Austenite grains that were revealed for each casting sample are shown in Figure 12. The images have been processed to further increase the clarity of the grains and include 0.25 in. (6.35 mm) scale bars for dimensional reference. Grain identification and analysis were performed on the images from Figure 12.

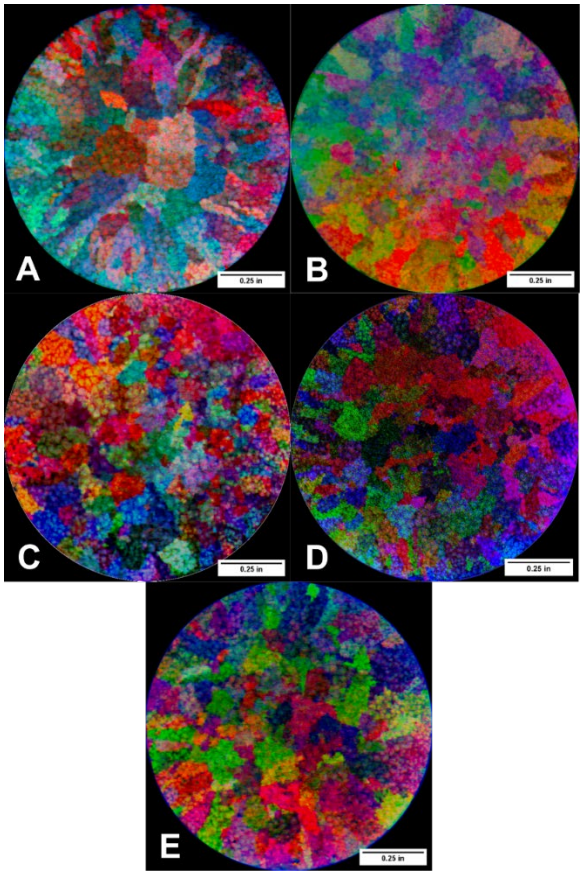

Figure 12. The macrographs of the austenite grains for each casting's sample: Si + Al (A), Si + Ca (B), Si + Ce/Mischmetal (C), Si + Sr (D), and Si + Ti (E). Each macrograph includes a scale bar to indicate 0.25 in. (6.35 mm).

Austenite grain size and count for equiaxed and columnar zones in all samples are listed in Tables 8-9. The same data is displayed visually in Figures 13-14. The sample with the Al in-mold addition was found to be an outlier in the values for grain size across all samples. For the additions of Ca, Ce, Sr, or Ti, the size of the austenite grains was relatively similar and fine sized in both the equiaxed and the columnar zone. However, the equiaxed zone of the Al sample had significantly larger and fewer equiaxed grains compared to the others. By comparison, the Ca sample had the highest grain count per area and the smallest average equiaxed grain size from the equiaxed zone data, 0.001 $in.^2$ (0.645 mm^2). The large difference between Al and Ca addition samples indicated the opposite effect of the two elements (at the chosen level of addition) on equiaxed austenite grain sizes. Data from columnar zones, however, did not show significant trends or outliers. This is possibly due to the thermal gradient being the dominant driver of columnar grain growth. It can also be seen that the number density of columnar grains does not seem to correlate to the grain sizes in the equiaxed zone.

Table 8. Austenite Grain Size for Both the Equiaxed and Columnar Zones in Different Castings

	Si +Al	Si +Ca	Si + Ce	Si + Sr	Si + Ti
Avg. Equiaxed Grain Size, $in.^2$ (mm^2)	0.008 (5.161)	0.001 (0.645)	0.003 (1.935)	0.002 (1.290)	0.002 (1.290)
Avg. Columnar Grain Size, $in.^2$ (mm^2)	0.002 (1.290)	0.003 (1.935)	0.003 (1.935)	0.002 (1.290)	0.003 (1.935)

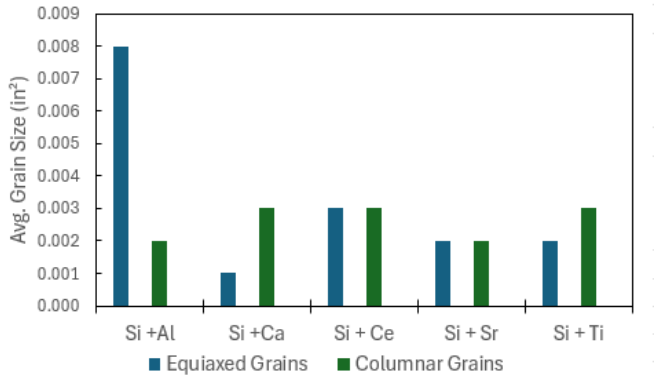

Figure 13. Austenite grain size for both the equiaxed and columnar zones in the different castings.

Table 9. Austenite Grain Count for Both the Equiaxed and Columnar Zones of Each Sample

	Si +Al	Si +Ca	Si + Ce	Si + Sr	Si + Ti
Equiaxed Grain Count, *#/in.²* (#/mm^2)	128.65 (0.19)	1195.80 (1.85)	391.19 (0.60)	408.89 (0.63)	429.00 (0.66)
Columnar Grain Count, *#/in.²* (#/mm^2)	438.89 (0.68)	348.79 (0.54)	348.05 (0.54)	406.25 (0.63)	301.84 (0.47)

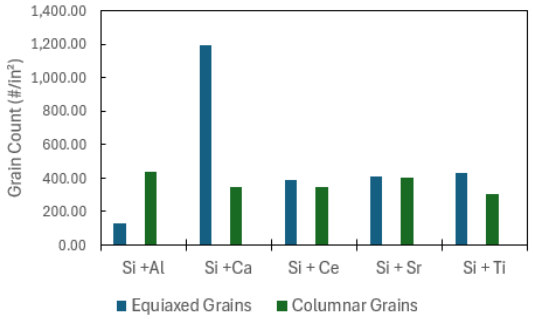

Figure 14. Austenite grain count for both the equiaxed and columnar zones of each sample.

For most castings, a larger equiaxed zone is preferred for isotropic properties. In Table 10 and Figure 15, area percentages of the equiaxed zone over the surface area examined are at two different levels across the samples. The Ce, Sr, and Ti samples all had roughly 50% of the surface examined covered by equiaxed grains. By comparison, the Al and Ca samples had 20% and 25%, respectively. It is also worth noting that the Ca sample had the finest equiaxed grains, but the Al sample had the largest equiaxed grains. A similar trend is seen with the average columnar grain length, as shown in Table 11 and Figure 16. The samples with a larger equiaxed zone also had significantly lower average columnar grain length.

Table 10. Equiaxed Zone Percentage for the Austenite Grains in Each Sample

	Si +Al	Si +Ca	Si + Ce	Si + Sr	Si + Ti
Equiaxed Area % ($in.^2/in.^2$)	20.920	25.310	52.850	54.050	46.800

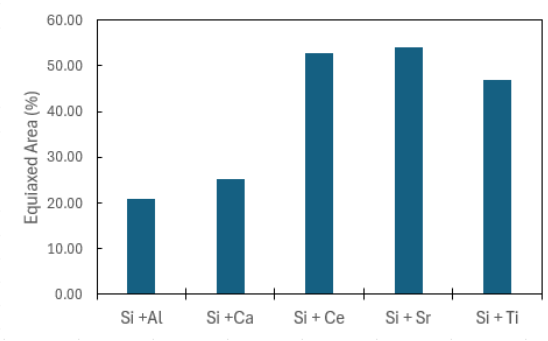

Figure 15. The equiaxed zone percentage for the austenite grains in each sample.

Table 11. Average Length for the Columnar Austenite Grains in Each Sample

	Si +Al	Si +Ca	Si + Ce	Si + Sr	Si + Ti
Avg. Columnar Grain Length, in. (mm)	0.314 (7.976)	0.291 (7.391)	0.159 (4.039)	0.154 (3.911)	0.185 (4.699)

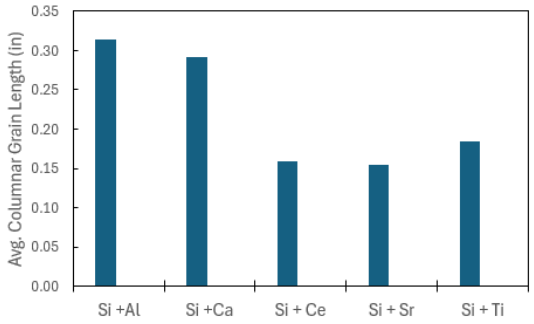

Figure 16. The average length for the columnar austenite grains in each sample.

EUTECTIC CELLS

The eutectic cells were successfully revealed after etching. During the process of measuring their sizes, it was apparent that there was a difference in the size of the eutectic cells within the equiaxed zone and the cells inside the columnar zone. Therefore, the two have been separated out to show that difference. The size of the eutectic cells in the columnar zones across all samples were similar, roughly 0.500 mm (0.020 in.). This again aligns well with the similar austenite grain sizes in columnar zone listed in Tables 8-9. It should be noted that the size of the eutectic cells in the equiaxed zone of samples with smaller equiaxed zones are also smaller. The Ca and Al samples both had smaller equiaxed zones, and the equiaxed zone eutectic cell diameters were 0.555 mm (0.021 in.) and 0.506 mm (0.019 in.) respectively. By comparison, the other samples have values over 0.600 mm (0.023 in.), as shown in Table 12 and Figure 17. This suggests a correlation between equiaxed eutectic cell diameter and equiaxed zone size, rather than the size of the austenite grains.

Table 12. Average Eutectic Cell Diameter for Each Sample in Both the Equiaxed Zone and Columnar Zone

	Si + Al	Si + Ca	Si + Ce	Si + Sr	Si + Ti
Equiaxed Zone – Avg. Eutectic Cell Diameter, *mm.* (*in.*)	0.506 (0.019)	0.555 (0.021)	0.629 (0.025)	0.731 (0.028)	0.739 (0.029)
Columnar Zone – Avg. Eutectic Cell Diameter, mm (in.)	0.536 (0.021)	0.482 (0.019)	0.503 (0.019)	0.512 (0.020)	0.566 (0.022)

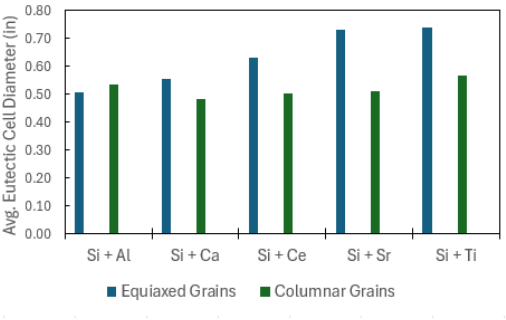

Figure 17. The average eutectic cell diameter for each sample in both the equiaxed zone and columnar zone.

RECOMMENDATION AND FUTURE WORK

Based on the experimental results for the different additions (addition rate at 0.05 wt.%) chosen for this study, the following results for austenite grain structure were obtained:

- Aluminum at 0.05 wt.% had the smallest equiaxed zone and the coarsest equiaxed grain structure.
- Ca at 0.05 wt.% had the finest equiaxed grain structure but may be at a cost of reducing the equiaxed zone.
- Sr of 0.05 wt.% mitigated the reduction of the equiaxed area while having a relatively fine structure.

The effectiveness of microstructure refinement, when multiple elements are added, needs to be further investigated. The potential impact on graphite formation with element additions will be investigated further in future studies.

CONCLUSIONS

The DAAS heat-treatment process retained the austenite grain structure in a gray iron alloyed with Ni and Mo. Five separate in-mold additions were studied and compared. At the addition rate of 0.05 wt.%, Al was found to have the smallest equiaxed zone area (~20 %), and largest equiaxed austenite grains. The Ca had a similarly small equiaxed zone area (~20 %), but the finest equiaxed austenite grains out of the five additions that were tested. The samples with the Ce (mischmetal), Sr, or Ti addition showed the largest equiaxed zones (~50 %), and similarly sized equiaxed austenite grains. Overall, all samples had similarly sized columnar zone austenite grains. The average diameter of the eutectic cells was measured for both the equiaxed zone and the columnar zone. The five samples had a similar average eutectic cell diameter in the columnar zone (~0.5 mm or 0.02 in.). However, the three samples with the larger equiaxed zone area had larger sized average equiaxed eutectic cells. This suggests a correlation between eutectic cell diameter and equiaxed zone.

ACKNOWLEDGMENTS

This work was from research projects funded by the American Foundry Society (AFS), 22-23#01 and the National Science Foundation (Award Number: 2301570). The authors also want to acknowledge the National Science Foundation (NSF) for supporting the research team to develop the macrostructure examination procedure, as well as acquiring the thermodynamic calculation software license used for alloy phase equilibrium calculation. The advisement of the AFS Research Committee and the AFS Cast Iron Research Division is greatly appreciated. Additionally, the undergraduate students, graduate students, and professors of the research team at Georgia Southern University are highlighted for their work and assistance with the research.

REFERENCES

1. Hussein Dhaher, N., *Materials Science and Engineering* (2019).
2. “Gray Iron,” *Metals Handbook Desk Edition* 309–314 (ASM International, 2018). doi:10.31399/asm.hb.mhde2.a0003107 (Link last accessed 02-11-25.)
3. “Microstructure and Characterization of High-Alloy Cast Irons,” *Cast Iron Science and Technology* 719–732 (ASM International, 2018). doi:10.31399/asm.hb.v01a.a0006351 (Link last accessed 02-11-25.)

4. Fourlakidis, V., Diószegi, A., Ribeiro, C.A.S. & Tekniska Hgskolan. Hgskolan i Jönköping. “Dendritic Morphology and Ultimate Tensile Strength of Pearlitic Lamellar Graphite Iron.”
5. Goodrich, G.M., “Introduction to Cast Irons,” *Casting* 785–811 (ASM International, 2018). doi:10.31399/asm.hb.v15.a0005322 (Link last accessed 02-11-25.)
6. “Microstructure Evolution during the Liquid/Solid Transformation in Cast Iron,” *Cast Iron Science and Technology,* 59–80 (ASM International, 2018). doi:10.31399/asm.hb.v01a.a0006304 (Link last accessed 02-11-25.)
7. Rivera, G., Calvillo, P.R., Boeri, R., Houbaert, Y. & Sikora, J., “Examination of the solidification macrostructure of spheroidal and flake graphite cast irons using DAAS and ESBD,” *Mater Charact* 59, 1342–1348 (2008).
8. López, M.G., Brewer, L.N., Massone, J.M., & Boeri, R.E., “EBSD Analysis of the Primary Austenite Grains in Lamellar Graphite Cast Iron,” *Metallography, Microstructure, and Analysis* 8, 386–392 (2019).
9. Arvola, D.A., “Grain Refinement of High Alloy Stainless Steels in Sand and Directionally Solidified Castings” (2018). https://scholarsmine.mst.edu/masters_theses/7793/ (Link last accessed 02-11-25.)
10. Li, Y., Bushby, A.J. & Dunstan, D.J., “The Hall-Petch effect as a manifestation of the general size effect,” *Proceedings of the Royal Society A: Mathematical, Physical and Engineering Sciences* 472 (2016).
11. “The Austenite-to-Ausferrite Transformation,” *Cast Iron Science and Technology*, 114–118 (ASM International, 2018). doi:10.31399/asm.hb.v01a.a0006319 (Link last accessed 02-11-25.)
12. Boeri, R.E., López, M.G., Tenaglia, N.E. & Massone, J.M., “Solidification of Ductile and Compacted Irons, Macrostructure and Shrinkage Formation,” *Int J. Metalcasting*, 14, 2020, 1172-1182.
13. Standard Specification for Gray Iron Castings 1, ASTM doi:10.1520/A0048_A0048M-03R16. (Link last accessed 02-11-25.)